Dynamic behaviors of fuel droplets impacting on the wall surfaces with different wettability and temperatures

Liang Guo[a], Yanling Chen[a], Ningning Cai[b], Wanchen Sun[a,*], Yuying Yan[c], Han Wang[a], Yuheng Gao[a]

[a] *State Key Laboratory of Automotive Simulation and Control, Jilin University, Changchun 130025, China*

[b] *School of Management, Jilin University, Changchun 130025, China*

[c] *Faculty of Engineering, University of Nottingham, Nottingham NG7 2RD, UK*

Abstract

To improve the controllability of combustion and reduce the emissions of HC and CO of the newly developed combustion modes, such as the HCCI, PCCI and RCCI, the evaporation processes and morphological developments of diesel droplets impacting on the aluminum alloy surfaces with different wettability and temperatures are experimentally investigated. The results show that the oleophilic surface is conducive to evaporation of diesel droplets, while the oleophobic surface promotes the formation of the vapor film between the fuel droplets and the test surface at a high surface temperature and reduces the Leidenfrost temperature of the fuel droplets. Also, stronger oleophobicity of the surface is beneficial to the rebound and secondary breakup of the droplets, thereby promoting the evaporation of the droplets in the gas-phase space of the cylinder and improving the air-fuel mixing. Moreover, the stronger the surface oleophobicity, the smaller the spreading factor and the larger the rebound factor of the droplets. At a higher wall temperature, the ability for enhancing the surface oleophobicity of the convex domes, grooves and protrusions structures on the laser-etched surface is better than that of the boss/pits and needle-like structures on the chemically etched surface. Under the conditions of lower surface temperatures, the evaporation rate of the droplet after hitting the wall is closely related to the spreading area of the droplet. As the wall temperature increases, when the droplet is in transition boiling regime, the large heat transfer rate makes the diffusion width, height and diffusion area of the vapor phase region are

* Corresponding author.
E-mail address: sunwc@jlu.edu.cn (W. Sun).

obviously large.

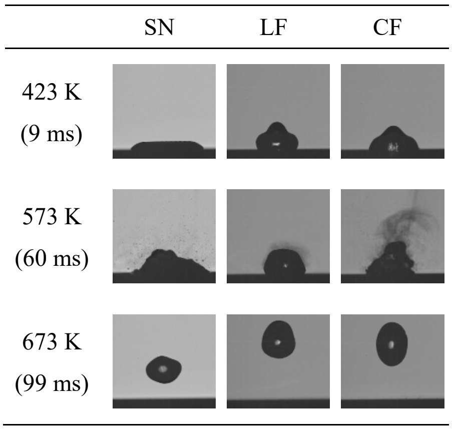

Graphical abstract

Keywords: Fuel droplet; Surface wettability; Wall temperature; Evaporation process; Morphological development

1. Introduction

Higher fuel economy and lower emission levels are the motivations for the development of vehicle engines. New combustion modes such as homogeneous charge compression ignition (HCCI) [1], premixed charge compression ignition (PCCI) [2], reaction controlled compression ignition (RCCI) [3] and low temperature combustion (LTC) [4,5] are promising combustion modes for improving engine performance and reducing emissions. Premixed compression ignition modes such as HCCI and PCCI are mostly low temperature combustion modes that use lean mixtures, and often use the early injection, the high pressure injection and the multiple injections to improve atomization quality [6-9]. Due to the low temperature and gas density at the early injection timing, the phenomenon of wall-wetting is inevitable [10]. Wall-wetting is one of the important sources of the soot particles and unburned hydrocarbons. Therefore, it is necessary to conduct an in-depth study on the fluid-solid interactions between the fuels and the combustion chamber walls to actively control the spreading, bouncing and vaporization behaviors of the fuel droplets. Since spray-wall impingement is a multi-scale and strong transient process, and there are many influencing factors, the mechanism of spray-wall impingement cannot be explained in detail. The research of the droplet-wall impingement is the basis of the study of the spray-wall impingement, and the wall-impinging droplet experiences dynamic behaviors (e.g. spreading, retraction, rebound, breakup, splashing) and thermodynamic behaviors (e.g. evaporation). Focusing on the droplet-wall impingement can highlight the influence of wall conditions, which is more conducive to exploring the fluid-solid coupling processes of droplet-wall impingement.

The research direction of the droplet-wall impingement has attracted attention for a long time. There are many factors that affect the dynamic processes of the wall-impinging droplets, and the influencing factors interact with each other [11]. With the development of material science and biomimetic science, specific wettability surfaces with micron-scale and nano-scale structures have been widely used [12], and the droplet behavior relates greatly to the apparent contact angle and the contact angle hysteresis [13]. Changing the geometrical sizes of the microstructures of the solid surfaces [14,15], adding coating [16-18] and modifing with low surface free energy material [19,20] can obtain surfaces with different wettability, such as superhydrophilicity, hydrophilicity, hydrophobicity and superhydrophobicity. Also, using a combination of masking, hydrophobic nanoparticle treatment and oxygen plasma treatment, the heterogeneous surfaces with moderate and extreme wettability contrasts are fabricated [21].

Many scholars have studied the movement and evaporation characteristics of the droplets after impacting on surfaces with different wettability and temperatures. At a room temperature, the wall wettability, physical and chemical properties of the droplets and Weber number have obvious effects on the spreading factor and apex height of the droplets impacting the walls with room temperature [22]. Similarly, the maximum spreading factor, spreading time and post-impact oscillation are also related to the above parameters [23]. The surface morphology could both suppress and facilitate drop splashing, and a method to predict splashing threshold on surfaces with different morphologies is presented [24]. When droplets hit the nano-textured superhydrophobic surfaces, the maximum spreading factor is related to $We^{0.52}$, and both of the contact time and non-dimensional contact time of bouncing droplets are independent of Weber number in the range of 1.5 to 121 [25]. When droplets impact obliquely on microstructured superhydrophobic surfaces, the increase in the normal Weber number leads to a transition from conventional retracting bouncing, to incomplete-retracting bouncing, and then to impaled retracting bouncing. With the increase of Ohnesorge number, the contact time shows a trend of "decrease"-"increase"-"decrease" [26].

At higher temperatures, Liang et al [27] conducted a comprehensive review of published literatures concerning the fluid mechanics and heat transfer mechanisms of liquid drop impact on a heated wall. The surface wettability, wall temperature, physical and chemical properties of the droplets and Weber number have effects on the boiling and evaporation characteristics of droplets impacting on the walls [28-30]. For various applications in energy systems, advanced thermal management solutions promoted the developments of the graphene functionalized coatings [31] and the specially treated wicks [32] in the field of phase-change heat transfer. Compared to the pristine rectangular microgrooves, the rectangular microgrooves with superhydrophilic nano-textured surfaces increase the axial wetting lengths of the fluids, which have a critical influence on the evaporating heat transfer [33]. In addition, the four stages of the impingement process are identified: impact, boiling, near constant surface diameter evaporation and final dry-out. And the nano-structured surface has a lower dissipated energy during impact and enhances the heat transfer for evaporative cooling with a 20% shorter time to achieve final dry out [34]. With the increase of the wall temperatures, the fuel droplets are in four different regimes, including film evaporation ($T_s \leq T_{sat}$, where T_s is the surface temperature and T_{sat} is the liquid saturation temperature), nucleate boiling ($T_{sat} \leq T_s \leq T_{chf}$, where T_{chf} is the temperature corresponding to the maximum heat flux), transition boiling ($T_{chf} \leq T_s \leq T_{Leid}$, where T_{Leid} is the liquid Leidenfrost temperature) and film boiling ($T_s \geq T_{Leid}$), respectively. When the droplets hit surfaces with the temperature higher than the Leidenfrost temperature of the droplets, the droplets are levitated upon the vapor layer resulting in a nonwetting state, which deteriorates the heat transfer [35-37]. This phenomenon is Leidenfrost phenomenon. However, water droplets can be suspended at the peaks of the roughness on a superhydrophobic interface, and vapor escapes from underneath the droplet, so a “pseudo-Leidenfrost” state appears for all excess temperatures [38]. The second fast spreading of the droplet resulting from vigorous boiling on the micro/nanostructured surfaces (ZnO nanowire surface and copper inverse opal surface) could enhance the heat transfer between the droplet and the surface and promote the Leidenfrost temperature of the impact droplet [39]. The Leidenfrost effect is closely related to practical applications. Recent studies with designed micropatterned surfaces were able to control the movement and evaporation of the Leidenfrost drop and change the drag [40-42]. For such applications, there are more efforts that focus on how to change the Leidenfrost temperature. Compared to smooth surfaces, surfaces with different textures can achieve a Leidenfrost temperature shift [43]. Micro/nano multiscale texture is the essential component in significantly increasing Leidenfrost temperature by inducing capillary wicking [44]. Some authors have reported that changing the surface roughness [45], the porous structure [46] and the nanofiber mats [47] could increase the Leidenfrost temperature. Also, as the hydrophilic surface causes vigorous nucleate boiling and large viscous dissipation during the droplet contact, higher the Leidenfrost temperature is required for stable film boiling state [48]. For rib-patterned superhydrophobic substrates, as the cavity fraction (relative projected cavity area of substrate to total projected surface area) increases, the heat transfer rate decreases, nucleate boiling is delayed to higher substrate temperatures and the Leidenfrost temperature reduces [49]. Other studies have found that enhancing surface hydrophobicity [50,51] could reduce the Leidenfrost temperature. Also, the dependence of the Leidenfrost temperature on the ambient conditions was investigated [52]. The increasing (decreasing) the ambient pressure lead to an increase (decrease) in Leidenfrost temperature. Increasing the ambient temperature stabilized meta-stable, levitating drops at increasingly lower temperatures below the Leidenfrost temperature. Besides the aforementioned experimental studies, some numerical researches on the processes of droplet-wall impingement are also performed to description of the complex problem involving both fluid mechanics and coupled heat and mass transfer [53-55].

So far, many researches related to the development processes of water droplets impacting on the surfaces have been reported. However, there are very few researches on the effects of the surface wettability on the behavioral development of fuel droplets hitting surfaces with high temperatures. Especially, the evaporation processes and morphological development processes of the wall-impinging fuel droplets containing multiple components at different wall temperatures have not been thoroughly explored. Aiming at the problem of wall-wetting during cold start of internal combustion engines, to realize the active control of the evaporation processes of the wall-wetting fuels under different wall conditions and improve the heat transfer efficiency in the heat transfer process, this research uses physical and chemical methods to reconstruct the microstructures of the aluminum alloy surfaces and fabricate surfaces with special wettability. High-speed photography and schlieren methods are used to study the evaporation processes and the morphological development processes of the liquid phase and the vapor phase after fuel droplets impact walls with special wettability under different wall temperature conditions. The comprehensive effects of surface wettability and wall temperature on heat exchange rates and evaporation processes of the droplets are analyzed. To improve heat transfer performance and reduce soot particles and unburned hydrocarbons, the results of this study will lay an experimental foundation for establishing active control methods of fuel evaporation, fuel-air mixture formation and combustion.

2. Experimental materials and methods

2.1. Experimental fuels and platforms

Diesel is selected as the test fuel. Diesel is mixtures of certain hydrocarbon compounds, and its physical and chemical properties are shown in **Table 1**.

Table 1 Characteristics of the tested fuel.

Properties	Diesel
Density /(kg·m^{-3})	821.9
Latent heat of vaporization /(kJ·kg^{-1})	251.2
Surface tension at 293 K /(mN·m^{-1})	29.3
Viscosity at 293 K /(mm^2·s^{-1})	4.07
Boiling point /(K)	453-623

Aluminum alloy is selected as the material of the test surface. The chemical compositions of the aluminum alloy used in the experiments are shown in the **Table 2**.

Table 2 Chemical compositions of aluminum alloy.

Element	Cu	Mn	Mg	Zn	Cr	Ti	Si	Fe	Al
Content /(%)	0.15-0.4	0.15	0.8-1.2	0.25	0.04-0.35	0.15	0.4-0.8	0.7	Margin

The microscopic morphologies of the metal surfaces are measured and recorded using Scanning Electron Microscope (SEM). The variations of the contact angles of the diesel droplets on the surfaces with time are recorded with the contact angle measuring instrument. A self-developed high-speed photography platform and a schlieren optical test platform are used to record the evaporation processes and morphological developments of the fuel droplets after impacting the surfaces. The evaporation times of the fuel droplets on the heated surfaces are recorded by a timer. The "z-type" layout scheme is selected for the schlieren optical test platform. The schematic diagrams of the above test platforms are shown in **Fig. 1**. The high-speed camera used in the experiments is a Phantom V611 high-speed camera. The practical resolution and shooting frequency selected for the present experiments are 512 pixels × 512 pixels and 1000 fps, respectively. The metal surface temperature is regulated and controlled with a self-developed temperature feedback measurement and control system. After calibration, the accuracy of the surface temperature is within 1 K. With a precise control knob, the droplet volume of each titration is controlled to 5 μL, with an error of no more than 1%.

(a) The high-speed photography platform

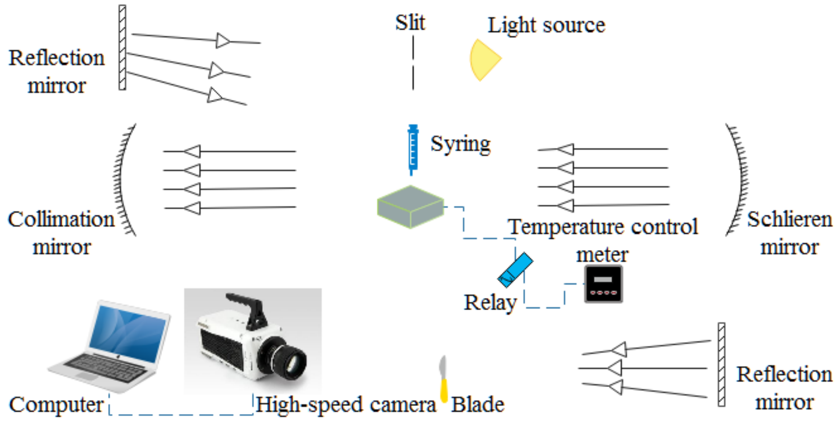

(b) The schlieren optical test platform

Fig. 1. Schematic diagrams of the test platforms.

2.2. Experimental surfaces

For the study of the contact angles and morphological developments of the liquid phase and gas phase of the droplets on the different surfaces, the sizes of the metal blocks are selected as 30 mm × 30 mm × 10 mm. However, to determine the evaporation times of the droplets, the sizes of the metal blocks are selected as 100 mm × 100 mm × 15 mm. A droplet in the Leidenfrost state tends to move around on the surface in a nearly frictionless manner. Therefore, a conical depression is machined with a 1° slope and a depth of 0.52 mm at the center of the test surface to keep the droplet from rolling off the test area.

The surface microstructures are reconstructed through laser etching and chemical etching. To avoid the influence of surface oxidation to the preparation of chemical etching, the in total six metal surfaces are pretreated with mechanical grinding and chemical cleaning. After mechanical grinding, the roughness of all the test surfaces is kept at 0.5 µm. The test substrates are further chemically cleaned using the ultrasonic cleaner with acetone, rectified ethanol and deionized water in sequence. After the pretreatment, different fabrication methods are used for different metal surfaces to complete the reconstruction of the surface microstructures. After micro fabrication, the metal surfaces with different microstructures are cleaned again with deionized water and rectified ethanol. To reduce the surface free energy, three of the metal surfaces are modified through surface free energy reduction method by immersing the test blocks into the ethanol solution of perfluorooctanoic acid (ESF) with a concentration of 0.03 mol/L, for an immersing time of 24 hours. The detailed information of the fabrication methods, together with the surface codes used in the experiments are given in **Table 3**.

Table 3 Fabrication methods of the metal surfaces.

	Fabrication methods	Modified with the ESF	Surface codes
Smooth surface	Not etched by other methods after pretreatment	No	SN
		Yes	SF
Laser etching	Pretreatment + laser etching	No	LN
		Yes	LF
Chemical etching	Pretreatment + 2.5 mol/L hydrochloric acid solution (10 min), boiling water (40 min)	No	CN
		Yes	CF

From a macro perspective, the orthogonal grid structure is seen on the laser-etched surface, and the labyrinth structure is observed on the chemically etched surface. To determine the microstructures of the surfaces obtained through different fabrication methods, the SEM photos of the test metal surfaces are taken as shown in **Fig. 2**.

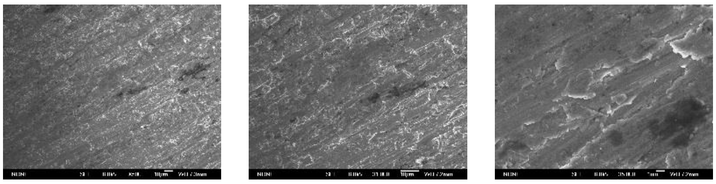

(a) Smooth surface (500× & 1000× & 5000×)

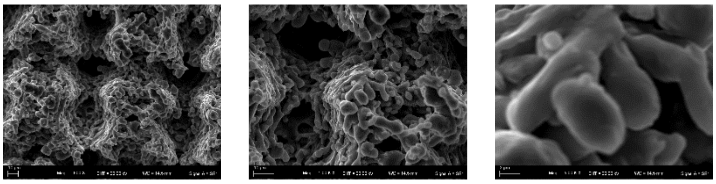

(b) Laser-etched surface (500× & 1000× & 5000×)

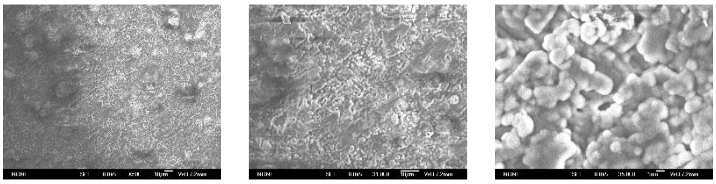

(c) Chemically etched surface (500× & 1000× & 5000×)

Fig. 2. SEM photos of the test surfaces.

Among the photos, **Fig. 2(b)** shows the SEM photos of the laser-etched surface. It can be seen from the figures that the micron-scale convex domes and grooves and the nano-scale protrusions are orderly formed by molten metal after laser etching. The size of a convex dome is about 80 μm × 100 μm. **Fig. 2(c)** shows the SEM photos of the chemically etched surface. After being etched by means of the hydrochloric acid solution immersion, the rectangular-shaped staggered cuboid boss/pits with a length and width of about 1-3 μm are formed upon the aluminum alloy surface. In addition, needle-like structures are formed through reaction between the aluminum alloy and the boiling water. The above two structures together form a good micro-nano interlaced structure on the aluminum alloy surface.

2.3. Data processing

To facilitate the analysis, the parameters relevant to morphological developments of both liquid phase and vapor phase of diesel droplets before and after it impacting on the walls are preliminarily defined, including the liquid phase spreading factor (d), the liquid phase rebound factor (h), the vapor phase diffusion width (W), the vapor phase diffusion height (H) and the vapor phase diffusion area (A). Among the parameters, d and h can be expressed as Eqs. (1) and (2).

$$d = d_i / d_0 \quad (1)$$

$$h = h_i / h_0 \quad (2)$$

Where, d_i is the spreading width of the droplet at the moment i after the diesel droplet impacts the wall. h_i is the vertical height between the highest point of the droplet and the wall at the moment i after the diesel droplet hits the wall. d_0 and h_0 are the droplet width (horizontal diameter) and height (vertical diameter), which are measured just before the first impact of the droplet, at the moment when the lower edge of the droplet is tangent to the wall. When the droplet rebounds against the surface without touching the surface, the spreading factor is 0. W is the width of the vapor phase diffusion along the wall surface after the impact. H is the height of the vapor phase diffusion in the direction perpendicular to the wall after the impact. A is the sum of the pixel area values included in the vapor phase measured from the schlieren images.

In order to make the measured droplet related physical parameters of this research have a higher accuracy, all the test results of the measured parameters are the averaged value of at least three measurements. All the calculated parameters are obtained from a self-developed image processing and calculation code. For the images obtained by high-speed photography, the parameters of the liquid phase of the wall-impinging droplets can be obtained through the steps of image reading, grayscale processing, background elimination, filtering, noise reduction, binarization and edge detection, etc. The schematic diagram of the process of the image processing of the liquid phase of droplets is shown in **Fig. 3**. The relevant parameters of the vapor phase after the fuel droplets hit the walls can be obtained by processing the images captured by the schlieren method. The schematic diagram of the image processing of vapor phase of the droplets is shown in **Fig. 4**. **Fig. 4(a)** is the original image of a single droplet hitting the wall obtained by schlieren method. Due to the opposite direction of the concentration gradient, it can be seen from the figure that there are obvious bright and dark areas on both sides of the droplet. The bright and dark areas are the vapor phase formed by the evaporation of the droplet. The area in the red circle in the middle of the image is the liquid phase of the droplet. According to different grayscale ranges, the bright and dark areas of the original image are extracted respectively. **Fig. 4(b)** is the extracted bright area and **Fig. 4(c)** is the extracted dark area. **Fig. 4(d)** is obtained by superimposing two grayscale images of **Fig. 4(b)** and **Fig. 4(c)**, removing background, and enhancing brightness. After filtering, noise reduction, binarization and other steps to obtain the final image **Fig. 4(e)**. In addition, according to the calibration, the relevant parameters of the vapor phase of the wall-impinging droplets can be calculated.

(a) (b)

Fig. 3. Schematic diagram of the image processing of liquid phase of the droplets.

(a) (b) (c) (d) (e)

Fig. 4. Schematic diagram of the image processing of vapor phase of the droplets.

3. Results and discussion

3.1. Effects of the surface microstructures and surface free energy on the wettability

The contact angle is one of the most important parameters in characterizing the wettability of a surface. **Fig. 5** shows the variations of the contact angles of diesel droplets on the six surfaces over time and the static visualization results of the droplets on the three surfaces modified with the ESF.

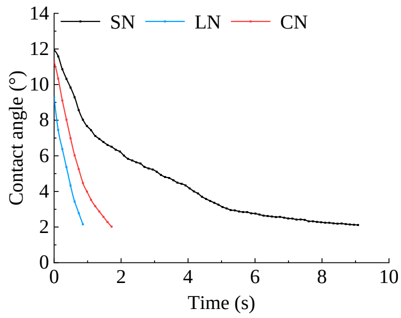

(a) Variations of the contact angles over time of the droplets on three surfaces without ESF modification

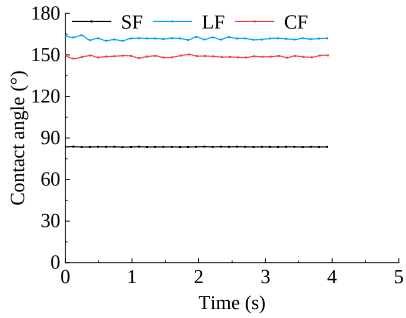

(b) Variations of the contact angles over time of the droplets on three surfaces modified with the ESF

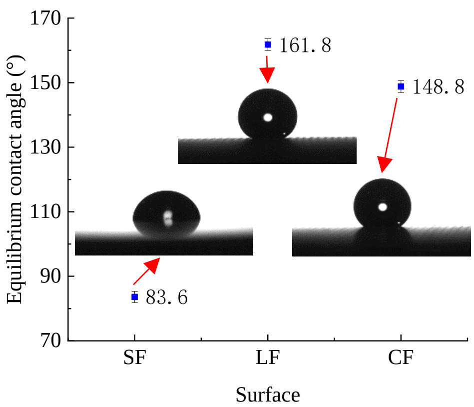

(c) Static visualization results of the droplets on the three surfaces modified with the ESF

Fig. 5. Contact angles of the diesel droplets on the surfaces with different wettability.

Fig. 5(a) shows the changing trends of the contact angles on the three different surfaces without surface free energy modification. It can be seen that all the three surfaces including the surfaces SN, LN and CN are oleophilic to diesel droplets. Compared with the smooth surface, the microstructures of the laser-etched surface and the chemically etched surface increase the surface roughness, and therefore, the oleophilicity of both the surface LN and the surface CN increase. The reduction rates of the contact angles of the diesel droplets on the surface LN and the surface CN are larger. Compared with the sizes of the cuboid boss/pits on the chemically etched surface, the sizes of the convex domes and grooves on the laser-etched surface are larger, and the interconnection between the intersecting grooves has an effect of promoting diversion of the fuel droplet, which makes the reduction rate of the contact angles of diesel droplet on the surface LN larger than that on the surface CN.

Fig. 5(b) shows the changing trends of the contact angles of diesel droplets on the three surfaces with different microstructures that are modified with ESF. It can be seen from **Fig. 5(b)** that the surface LF and the surface CF are more oleophobic to diesel droplets, compared with the smooth surface. After being modified with the ESF, the oleophobicity of the surface is found increasing with the increase of the surface roughness. As a result, the contact angle of the diesel droplet on the surface LF is largest among all the three ESF modified surfaces.

Fig. 5(c) shows the static visualization results of diesel droplets on the surfaces SF, LF and CF. Depending on the surface wettability, the equilibrium shapes of droplets vary. The intrinsic contact angles obtained on the surface SF is 83.6°, and the apparent contact angles obtained on the surface LF and the surface CF are 161.8° and 148.8°, respectively, which are determined by the characteristics of the solid-liquid-gas three-phase composite contact surface formed between the liquid and the solid surface. The Cassie-Baxter equation is as follows:

$$\cos\theta_c = f_1 \cos\theta - f_2 \tag{3}$$

$$f_1 + f_2 = 1 \tag{4}$$

Where, θ_c is the apparent contact angle of the droplet on the rough surface. θ is the intrinsic contact angle of the drop on the smooth surface. f_1, f_2 are the proportions of the solid-liquid contact surface and the gas-liquid contact surface in the composite contact surface, respectively. According to the results calculated with the Cassie-Baxter equation, the proportions of the solid-liquid contact surface in the composite contact surface are 4.5% and 13.0% for the surface LF and the surface CF, respectively. That is, the convex domes, grooves and protrusions structures on the laser-etched surface have a stronger ability to trap the air than the boss/pits and needle-like structures on the chemically etched surface.

3.2. Effects of the surface wettability on the Leidenfrost temperature of the droplets

For internal combustion engines, the wall temperatures of the combustion chamber could vary over a wide range under different operating conditions. To study the effects of the surface wettability on the Leidenfrost temperature of the wall-impinging fuel droplets, the evaporation times of the diesel droplets after impacting the different surfaces are investigated. The evaporation times of diesel droplets hitting surfaces with different wettability and temperatures are recorded. The Leidenfrost temperature of the droplet is determined by the method of droplet evaporation time. **Fig. 6** shows the Leidenfrost temperature of diesel droplets on the different surfaces. In the figure, CA is the abbreviation of contact angle.

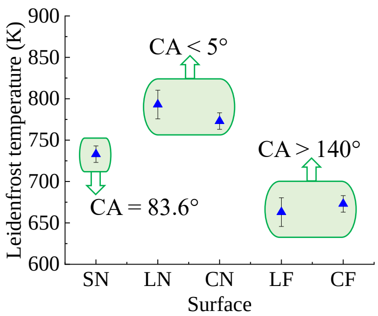

Fig. 6. Leidenfrost temperature of the droplets on different surfaces.

It can be seen from **Fig. 6** that diesel droplets have the highest Leidenfrost temperature on the surface LN among the three oleophilic surfaces. This is mainly because the roughness of the surface LN is the largest, and the microstructures are easier to pierce the vapor film formed between the droplets and the solid surfaces. Therefore, the droplets are in direct contact with the surfaces, and due to the rapid heat exchange, the droplets are disturbed by the fuel vapor escaped from three-phase contact surfaces. That is, when a droplet hits an oleophilic surface with a larger roughness, a higher surface temperature is required to produce a sufficiently stable vapor layer to make the droplets are in film boiling regime. The formation of the vapor layer is related to the nucleation, growth and merging of vapor bubbles. The Leidenfrost temperature of fuel droplets on the oleophilic and oleophobic surfaces is different, which can be attributed to the following aspects. On the oleophilic surfaces, the spreading areas of the droplets are larger and the liquid films are thinner. At the same time, isolated bubbles are difficult to merge and the bubbles easily penetrate the free surfaces of the liquid films. However, on the oleophobic surfaces, the bubbles are easy to merge, which facilitates the formation of the vapor layer. Furthermore, when droplets hit oleophobic surfaces, the potential barrier for the transition to film boiling is smaller, which makes it easier for droplets to enter film boiling regime on oleophobic surfaces. It suggests that the stronger oleophobic the surfaces, the lower the Leidenfrost temperature of the droplets. As a result, the Leidenfrost temperature of the droplets on the surface LF with the strongest oleophobicity is the lowest.

3.3. Effects of the surface wettability on the morphological development of the liquid phase of the droplets at different wall temperatures

To deeply understand the influence mechanisms of the surface wettability and wall temperature on the morphological developments of the liquid phase of the wall-impinging fuel droplets in four different regimes, the development characteristics of the diesel droplets after impacting the different surfaces are investigated. The surfaces SN, LF and CF shown in **Table 3** are used as the surfaces for the test. Four typical wall temperatures of 423 K, 473 K, 573 K and 673 K are investigated. The morphological development of the liquid phase of the droplets are studied with a droplet titration height of 10 mm. The visualization results are shown in **Fig. 7**.

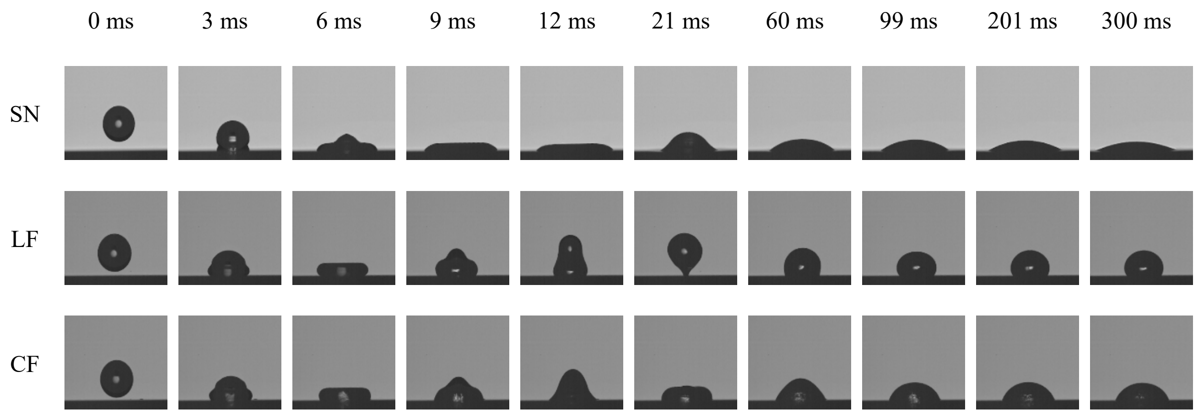

(a) 423 K

0 ms 3 ms 6 ms 9 ms 12 ms 21 ms 60 ms 99 ms 201 ms 300 ms

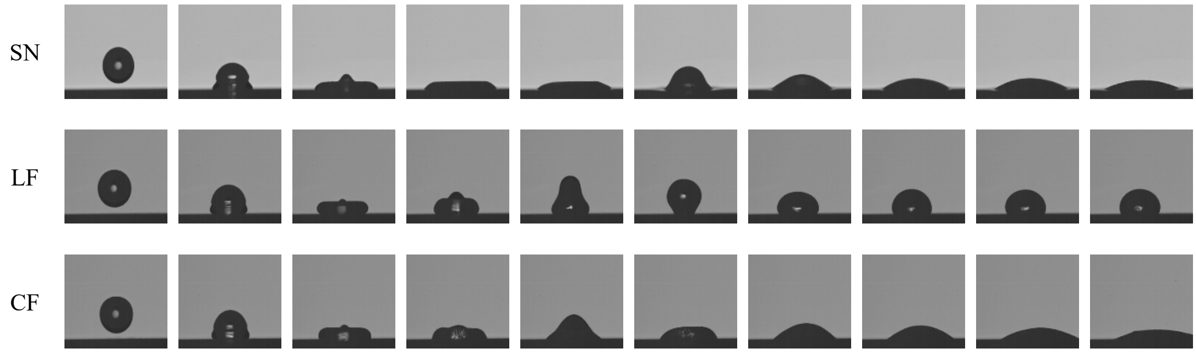

(b) 473 K

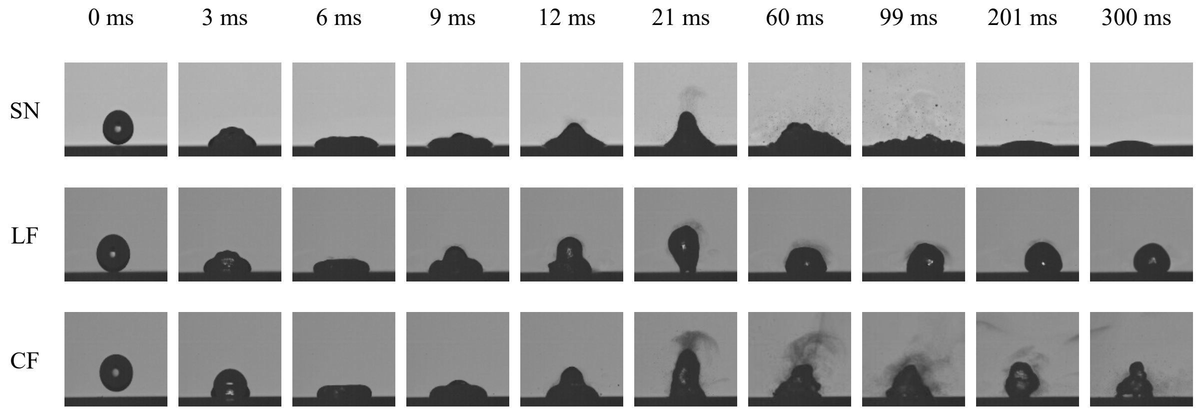

(c) 573 K

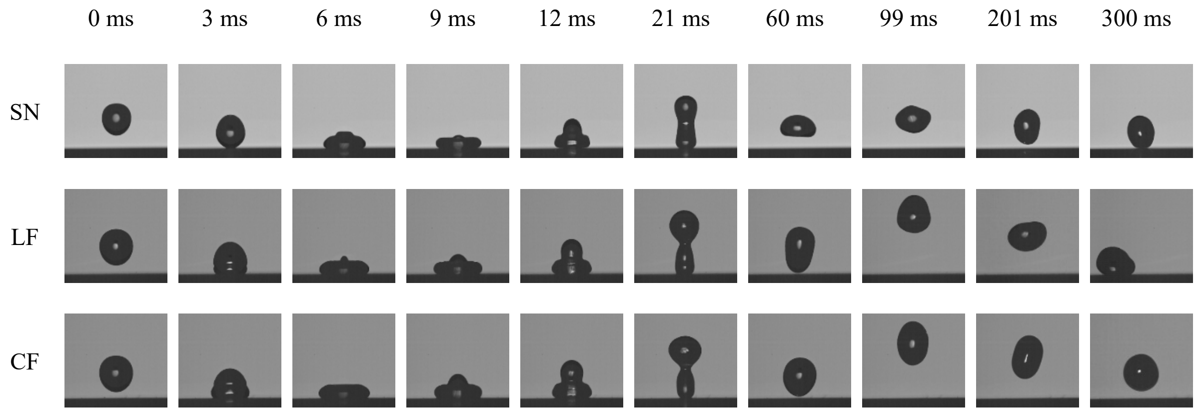

(d) 673 K

Fig. 7. Morphological developments of the liquid phase of the droplets after impacting on the different surfaces.

It can be seen in **Fig. 7** that the morphological developments of the fuel droplets after impacting on the oleophobic surfaces are significantly different, due to the different surface temperatures. At the wall temperature of 423 K, as seen in **Fig. 7(a)**, the diesel droplet is in the film evaporation regime. At 9 ms, the heat transfer performance is better on the surface SN with thinner liquid film than that on the surfaces LF and CF. Interestingly, at 12 ms, when the droplet shows the "disc-like" appearance on the surface SN, they appear as "gourd-like" and "mountain-like" shapes on the other two surfaces, LF and CF, respectively. Among the three surfaces, the oleophobicity of the surface LF is the strongest one. As it can be seen, at about 21 ms after collision, the droplet rebounds against the surface LF.

At the wall temperature of 473 K, the wall temperature reaches the boiling temperature of some components of the fuel that have a low boiling point, such as alkanes, cycloalkanes and aromatics with low carbon numbers. At the same time, the viscosity and the surface tension of the droplets decrease with the increased surface temperature. It can be seen from **Fig. 7(b)** that at 9 ms, compared with the photos taken at the wall temperature of 423 K, the spreading widths of droplets on the surface LF and the surface CF are larger under the wall temperature of 473 K, particularly on the surface CF after 21 ms of collision.

At the wall temperature of 573 K, steam appeared above the droplets can be seen clearly in **Fig. 7(c)**, that is generated due to the high surface temperature, especially at and after 21 ms of collision to the surface LF and the surface CF. Remarkably, the behaviors of the droplets impacting on the surfaces with different wettability are various. On the oleophilic surface, small splashes of liquid are clearly observed on the upper surface of the liquid after the collision. This is mainly due to the venting of the vapor bubbles. After the droplets hit the oleophobic surfaces, the droplets are disturbed by the fuel vapor escaped from three-phase contact surface, which makes the shapes of the droplets complex. The contours of the droplets are irregular and jagged, as shown in **Fig. 7(c)**. The surfaces with a stronger oleophobicity promotes the rebound of the droplets against the surface and makes it easier for the droplets to be in film boiling regime, which is consistent with the previous conclusions.

At the wall temperature of 673 K, as seen in **Fig. 7(d)**, due to the unstable vapor film, the droplet on the surface SN has a tendency to rebound off the surface, and when the vapor film becomes more stable as the wall temperature rises, the droplet will be in film boiling regime. However, on the two oleophobic surfaces, due to the metal surface temperatures is much higher than the boiling point of all the diesel components, and the stable vapor films prevent the direct liquid-solid contact, the diesel droplets are in film boiling regime. The droplets on the above two surfaces are supported by the vapor films, so the heat flux significantly reduce. As a result, the fuel droplets will no longer wet the walls after hitting them, but will behave as periodic beating until they are completely evaporated.

The behaviors related to the morphological development process of the fuel droplets due to injection within the internal combustion engines mainly include spreading, rebounding, splashing and secondary breakup. To quantify and compare the effects of surface wettability and wall temperature on the behavioral developments of the droplets, such as spreading and rebound, after hitting the walls, the spreading factor and rebound factor of the droplets under different wall conditions are measured and compared to each other, as shown in **Fig. 8** and **Fig. 9**.

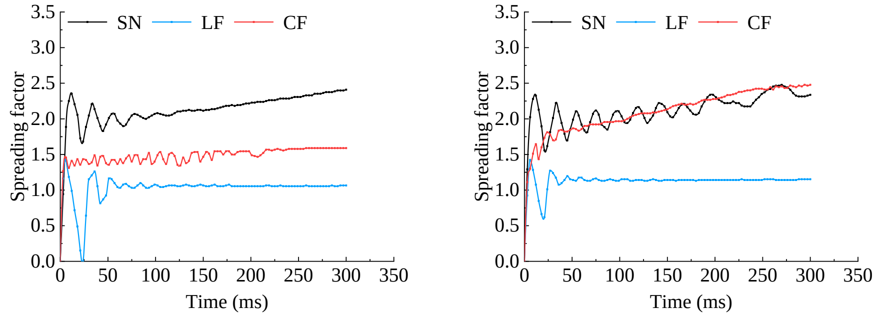

(a) 423 K (b) 473 K

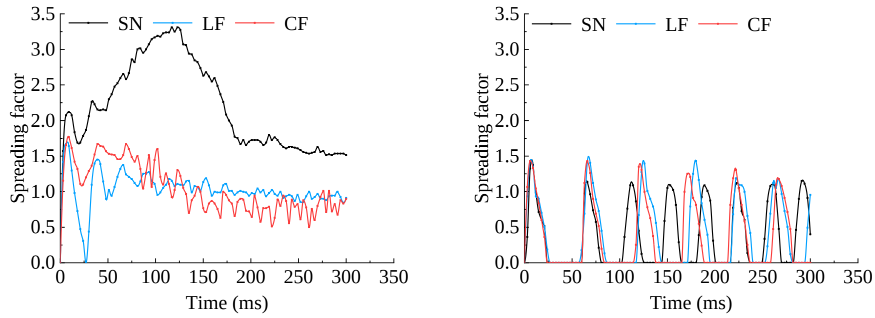

(c) 573 K (d) 673 K

Fig. 8. Effects of the surface wettability and wall temperature and on the spreading factor of the droplets.

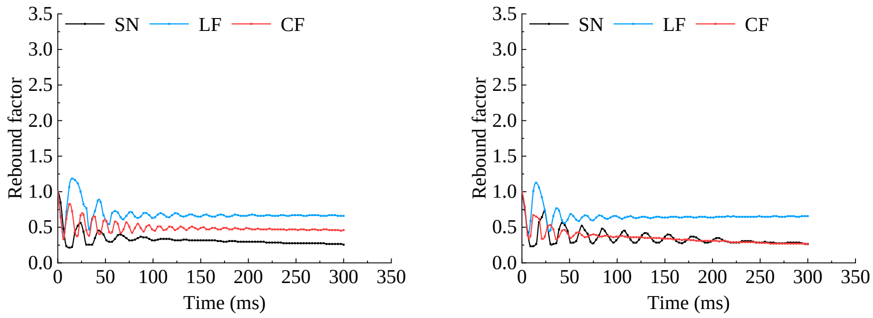

(a) 423 K (b) 473 K

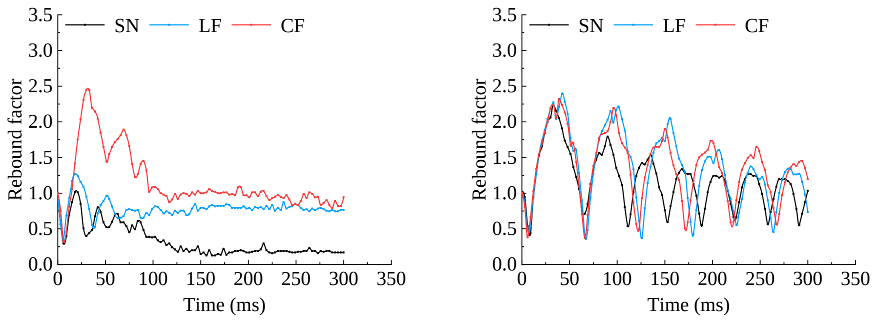

(c) 573 K (d) 673 K

Fig. 9. Effects of the surface wettability and wall temperature on the rebound factor of the droplets.

Generally, at lower surface temperatures, e.g. 423 K and 473 K, the smooth surface SN presents a higher spreading factor and a lower rebound factor compared to the surface LF and the surface CF. While, the laser etched surface with a surface free energy modification shows a lower spreading factor but a higher rebound factor compared to the other two surfaces. The above results are attributed to the smaller energy required for rebounding on the oleophobic surfaces. At the surface temperature of 423 K, the maximum rebound factor of the fuel droplets on the surface LF reaches 1.18, and the spreading factor is 0.72 at this moment. These results indicate that at a lower surface temperature condition, the oleophobic surface is more conducive to the rebound rather than spreading of the fuel droplets.

When the surface temperature is 473 K, comparing to the surface temperature of 423 K, it can be seen that the variations of both the spreading factor and rebound factor on the surface SN are more significant. At the same time, the spreading factor and the rebound factor on the surface CF are found to be increased and decreased, respectively, due to the increase in the surface temperature. It makes the value of these two parameters on the surface CF closer to that of the surface SN. The changes in spreading factor and rebound factor are mainly the results of the decrease in the viscosity and surface tension of the fuel droplets caused by the increased surface temperature. In addition, the result indicates that the ability of convex domes/grooves and protrusions structures on the laser-etched surface for enhancing the oleophobicity is better than that of the boss/pits and needle-like structures of the chemically etched surface.

With a further increase of surface temperature to 573 K, the variation amplitude of both the spreading factor and the rebound factor on all the three surfaces become higher, especially in the short period right after hitting the walls. As mentioned in the previous section, the surface LF and the surface CF has stronger oleophobicity than the surface SN, and the high oleophobicity of the both surfaces can be kept at a higher surface temperature. As a result, after hitting the surface LF and the surface CF, the droplets can still keep a very small spreading area which is also the evaporation area. Although both viscosity and surface tension of the droplets are decreased after impacting on the high temperature surfaces, it seems that the wettability of the surface is not influenced significantly by the surface temperature when it is 573 K.

At the surface temperature of 673 K, as shown in **Fig. 8(d)** and **Fig. 9(d)**, it can be seen that both the spreading factor and rebound factor of the droplets present clear changes compared with that on the three surfaces with lower temperatures. The most important change is that under the surface temperature of 673 K, the two factors both show periodic fluctuations with obvious regularity. This is mainly because at the excessively high surface temperature, the vapor film formed between the hot surface and the droplet lifts the droplet periodically and prevents the direct contact between the droplet and the surface. As a result, the fuel droplets on all the surfaces exhibit similar behaviors, that is, the droplets are not able to spread stably on the surface when the surface temperature is about the Leidenfrost temperature. It indicates that when the wall temperature is higher than the Leidenfrost temperature of the droplets, the effects of the surface wettability on the morphological development of the wall-impinging droplets are significantly weakened.

3.4. Effects of the surface wettability on the morphological development of the vapor phase of the droplets at different wall temperatures

To further understand the performance of wettability and wall temperature in improving the fuel evaporation, the morphological development processes of both liquid and vapor phases of diesel droplets impacting on the different surfaces are investigated with schlieren method. The wall temperatures used for the experiment are 423

K, 473 K, 573 K and 623 K, respectively. The surfaces SN, LN and CF are used as the test surfaces. The titration height of 15 mm for the droplet is used which is higher than that of the experiment introduced in last section. The schlieren visualization results of the morphological development of the both liquid and vapor phases are shown in **Fig. 10**.

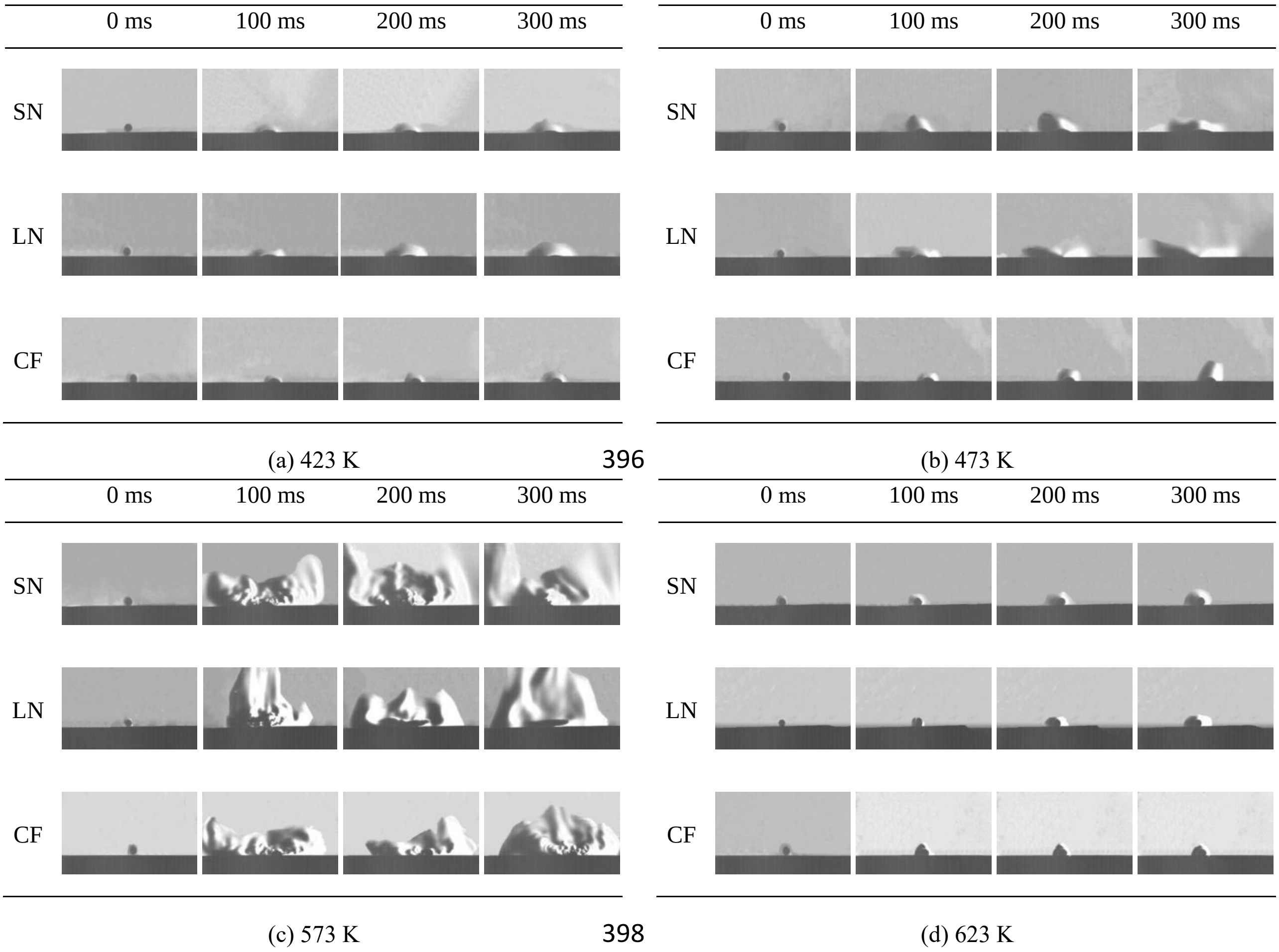

Fig. 10. Morphological developments of the liquid and the vapor phases.

Fig. 10(a) shows the imaging results of the droplets hitting the surfaces with different wettability at a wall temperature of 423 K. Compared to the images obtained at higher wall temperatures as shown in **Fig. 10(b)** and **Fig. 10(c)**, it can be found that at a wall temperature of 423 K, the diffusion rates of the vapor phase of diesel on all the three surfaces are slower. It can also be seen that among all the three surfaces, the smallest vapor diffusion area appears on the surface CF which has strongest oleophobicity, while the largest vapor diffusion area appears on the surface LN of which the oleophilicity is strongest among all the surfaces. It suggests that under the conditions of lower surface temperatures, the vapor phase diffusion area of the droplet after hitting the wall is closely related to the spreading area of the droplet. The larger the spreading area, the faster the evaporation rate of the fuel.

At a wall temperature of 473 K, after the droplets impac on all the three surfaces the walls, the heat transfer modes between surfaces and droplets are heat conduction. The evaporation rate is seen higher than that at the wall temperature of 423 K. It can be seen from **Fig. 10(b)** that during the development of the vapor phase, the maximum diffusion width of vapor phase of diesel appears on the surface LN. This is mainly because, on the one hand, the increase in surface temperature reduces the viscosity of the fuel and makes it easier to obtain a greater spreading area. On the other hand, the laser-etched orthogonal groove structure on the surface has a strong diversion effect on the fuel droplet, so that after hitting the wall, a larger spreading area and a thinner fuel film thickness can be obtained, which is conductive to the escape of bubbles from the surface of the fuel film and promote heat transfer. For the surface CF, it has been verified from the test results that the oleophobicity of the surface can be well maintained at a wall temperature of 473 K. Because of the smaller spreading area as well as the smaller heat exchange area of the droplet on the surface CF, the heat transfer to the droplet and evaporation rate of it will also be smaller.

As is evident in above images, when the wall temperature rises to 573 K, the degree of the vapor phase diffusion is significantly enhanced, and the diffusion area is obviously larger than that of the results obtained at the other three wall temperatures. This is mainly because at 573 K, the wall temperature has reached the boiling temperature of most components of the fuel components, but has not yet reached the Leidenfrost temperature of them. Under such condition that the stable vapor film has not yet formed, the droplet will not detach from the surface after hitting the wall, but the heat transfer rate between the surface and the droplet is larger due to the increased temperature difference between the two, leading to the immediately boiling and quick evaporation of the fuel droplet right after it hits the wall. It implies that, compared with the surface temperature, the wall wettability has little effect on the droplet evaporation rate at the condition that the droplet is in the transient boiling regime.

Fig. 10(d) shows that when the wall temperature reaches 623 K, due to combined effect of the lift force of the vapor film and the wall reaction force, the fuel droplets partially wet the metal surfaces after hitting the walls. Also, the partial nonwetting results in less energy dissipation, which causes the droplets to gain more kinetic energy to retract and tend to rebound and fall periodically. Furthermore, as the temperature rises from 573 K to 623 K, the low thermal conductivity of the vapor film inhibits heat transfer between the hot surface and the droplet. As a result, when the wall temperature rises to 623 K, the evaporation amount of droplets on all the three surfaces are reduced compared with that at the surface temperature of 573 K, for all the time intervals after hitting the walls.

Based on the imaging results, the width, height and the two-dimensional area value of the vapor phase region perpendicular to the camera direction are quantified at different moments after droplet-wall impingement through the method of pixel point progressive scanning, as shown in the **Fig. 11**.

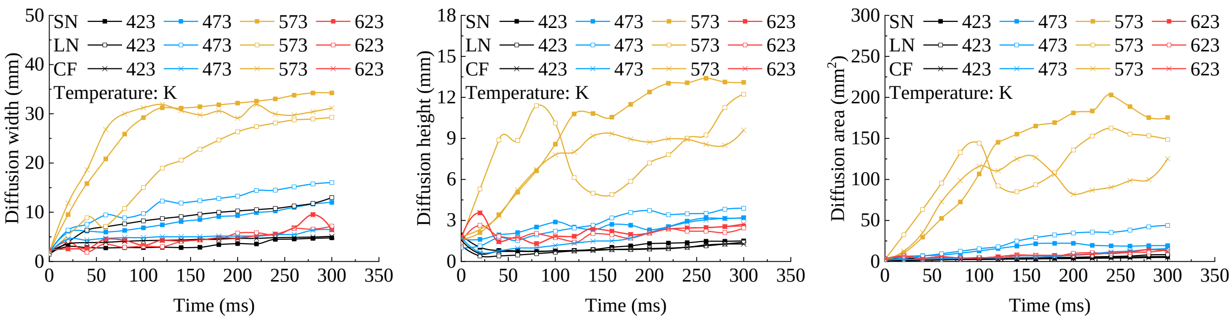

(a) The changes of W over time (b) The changes of H over time (c) The changes of A over time

Fig. 11. Effects of the surface wettability and wall temperature on W, H, A.

It can be seen from **Fig. 11** that when the wall temperature is 573 K, the diffusion width, height and area of the vapor phase region are obviously larger than those under the other three wall temperature conditions. This is mainly because the larger heat transfer rate at 573 K makes the evaporation rate of the droplet at this surface temperature is clearly larger than the results obtained under other surface temperature conditions.

At the surface temperature of 473 K, it is noted that the maximum values of the three geometric parameters of the evaporation region are all contributed by the surface LN, as seen in **Fig.11**. At the wall temperature of 473 K, the evaporation rate is closely related to the spreading area of the droplet. Referring to the imaging results of **Fig. 10**, it can be seen that after impacting the wall, affected by the wettability and micro-morphology of the surfaces, the spreading area of the droplet on the surface LN is largest among all the three surfaces, resulting in a greater evaporation rate of the surface LN, comparing to that of the other two surfaces.

In addition, **Fig. 11** shows that at the wall temperature of 423 K and 623 K, the width, height and area of the evaporation region in different time intervals after droplet-wall impingement are significantly smaller than those obtained at the other two surface temperatures. However, the reasons for the small evaporation rates under the surface temperatures of 423 K and 623 K are different. When the wall temperature is 423 K, the main reason for the small evaporation rate is the small temperature difference between the surfaces and the droplets. Although the surface wettability has a notable effect on spreading area of the droplets after hitting the walls, it has less influence on the evaporation rate of the droplets due to the low heat transfer rate between the surfaces and the droplets which is caused by the low wall temperature of all the three test surfaces. While on the surfaces of 623 K, the vapor film between the droplets and the wall surfaces is the main reason that affects the evaporation rate of the droplets, indicating that when the wall temperature is near the Leidenfrost temperature of the fuel, the vapor film causes a significant drop in fuel evaporation rate. However, in the actual application of the engines, if the droplets hit vertically a surface such as the cylinder wall, the film boiling caused by the high surface temperature could be beneficial to the rebound and secondary breakup of the fuel droplets, thereby promoting the evaporation of the droplets in the gas-phase space of the cylinder and improving the air-fuel mixing.

4. Conclusions

The aluminum alloy surfaces with different microstructures and special wettability are fabricated with the methods of laser etching, chemical etching and surface free energy modification. Using the high-speed photography and the schlieren methods, the morphological development process of both liquid phase and vapor phase of the diesel droplets together with the evaporation process after the droplets impact on the surfaces with different wettability and temperatures are experimentally investigated. The main conclusions can be summarized as follows:

(1) Depending on the surface microstructures and surface free energy, the contact angle of diesel droplets on the laser-etched oleophilic surface is the smallest, and the contact angle on the laser-etched oleophobic surface modified with the ESF is the largest among the all test surfaces.

(2) When the droplets hit oleophilic surfaces, the larger the roughness, the faster the evaporation rate at low wall temperatures. Stronger oleophobicity of the surface reduces the Leidenfrost temperature of the fuel droplets, and makes it easier for the droplets to be transferred to the film boiling regime, thereby promoting the evaporation of the droplets in the gas-phase space of the cylinder and improving the air-fuel mixing.

(3) Compared with the spreading behavior, the oleophobic surface facilitates the rebound of the droplets. When the wall temperature exceeds the Leidenfrost temperature of the droplet, the influence of the surface wettability on the morphological development of the droplet after the droplet-wall impingement is significantly weakened.

(4) Under the lower surface temperatures, the vapor phase diffusion area of the droplet after collision is closely related to the spreading area of the droplet. The larger the spreading area, the better the heat transfer performance and the faster the evaporation rate of the fuel. When the droplet is in transition boiling regime, the large heat transfer rate makes the diffusion width, height and diffusion area of the vapor phase region are obviously large.

Notes

The authors declare no competing financial interest.

Acknowledgments

The authors gratefully acknowledge the financial support from the National Natural Science Foundation of China (Project code: 51676084), Jilin Province Science and Technology Development Plan Project (Project code: 20180101059JC), Jilin Province Specific Project of Industrial Technology Research & Development (Project code: 2020C025-2) and Jilin University Ph.D. Interdisciplinary Research Funding Project (Project code: 101832020DJX041).

The authors gratefully acknowledge the financial support from the National Natural Science Foundation of China (Project code: 51676084), Jilin Province Specific Project of Industrial Technology Research & Development (Project code: 2020C025-2), Jilin University Ph.D. Interdisciplinary Research Funding Project (Project code: 101832020DJX041) and 2021 "Interdisciplinary Integration and Innovation" Project of Jilin University (Project code: XJRCYB07).

References

[1] M.M. Hasan, M.M. Rahman, Homogeneous charge compression ignition combustion: Advantages over compression ignition combustion, challenges and solutions, Renew Sust Energ Rev, 57 (2016) 282-291. https://doi.org/10.1016/j.rser.2015.12.157

[2] R. Kiplimo, E. Tomita, N. Kawahara, S. Yokobe, Effects of spray impingement, injection parameters, and EGR on the combustion and emission characteristics of a PCCI diesel engine, Appl Therm Eng, 37 (2012) 165-175. https://doi.org/10.1016/j.applthermaleng.2011.11.011

[3] J. Benajes, A. Garcia, J. Monsalve-Serrano, V. Boronat, Achieving clean and efficient engine operation up to full load by combining optimized RCCI and dual-fuel diesel-gasoline combustion strategies, Energy Conv. Manag., 136 (2017) 142-151. https://doi.org/ 10.1016/j.enconman.2017.01.010

[4] A.K. Agarwal, A.P. Singh, R.K. Maurya, Evolution, challenges and path forward for low temperature

combustion engines, Progress In Energy And Combustion Science, 61 (2017) 1-56. https://doi.org/10.1016/j.pecs.2017.02.001

[5] M. Krishnamoorthi, R. Malayalamurthi, Z.X. He, S. Kandasamy, A review on low temperature combustion engines: Performance, combustion and emission characteristics, Renew Sust Energ Rev, 116 (2019). https://doi.org/10.1016/j.rser.2019.109404

[6] M.P.B. Musculus, P.C. Miles, L.M. Pickett, Conceptual models for partially premixed low-temperature diesel combustion, Progress In Energy And Combustion Science, 39 (2013) 246-283. https://doi.org/10.1016/j.pecs.2013.12.001

[7] A.K. Agarwal, A. Dhar, J.G. Gupta, W.I. Kim, K. Choi, C.S. Lee, S. Park, Effect of fuel injection pressure and injection timing of Karanja biodiesel blends on fuel spray, engine performance, emissions and combustion characteristics, Energy Conv. Manag., 91 (2015) 302-314. https://doi.org/10.1016/j.enconman.2014.12.004

[8] W. Du, Q.K. Zhang, W.H. Bao, J.J. Lou, Effects of injection pressure on spray structure after wall impingement, Appl Therm Eng, 129 (2018) 1212-1218. https://doi.org/10.1016/j.applthermaleng.2017.10.083

[9] S. Polat, An experimental investigation on combustion, performance and ringing operation characteristics of a low compression ratio early direct injection HCCI engine with ethanol fuel blends, Fuel, 277 (2020). https://doi.org/10.1016/j.fuel.2020.118092

[10] H. Bendu, S. Murugan, Homogeneous charge compression ignition (HCCI) combustion: Mixture preparation and control strategies in diesel engines, Renew Sust Energ Rev, 38 (2014) 732-746. https://doi.org/10.1016/j.rser.2014.07.019

[11] X.J. Yu, Y. Zhang, R. Hu, X.B. Luo, Water droplet bouncing dynamics, Nano Energy, 81 (2021). https://doi.org/10.1016/j.nanoen.2020.105647

[12] Y.H. Sun, Z.G. Guo, Recent advances of bioinspired functional materials with specific wettability: from nature and beyond nature, Nanoscale Horizons, 4 (2019) 52-76. https://doi.org/10.1039/c8nh00223a

[13] F.Q. Chu, X.M. Wu, Q. Ma, Condensed droplet growth on surfaces with various wettability, Appl Therm Eng, 115 (2017) 1101-1108. https://doi.org/10.1016/j.applthermaleng.2017.01.060

[14] S.Y. Misyura, G.V. Kuznetsov, D.V. Feoktistov, R.S. Volkov, V.S. Morozov, E.G. Orlova, The influence of the surface microtexture on wettability properties and drop evaporation, Surf Coat Tech, 375 (2019) 458-467. https://doi.org/10.1016/j.surfcoat.2019.07.058

[15] D. Song, B.W. Song, H.B. Hu, X.S. Du, Z.B. Ma, Contact angle and impinging process of droplets on partially grooved hydrophobic surfaces, Appl Therm Eng, 85 (2015) 356-364. https://doi.org/10.1016/j.applthermaleng.2015.03.071

[16] E. Taghvaei, A. Moosavi, A. Nouri-Borujerdi, M.A. Daeian, S. Vafaeinejad, Superhydrophobic surfaces with a dual-layer micro- and nanoparticle coating for drag reduction, Energy, 125 (2017) 1-10. https://doi.org/10.1016/j.energy.2017.02.117

[17] Hooda, M.S. Goyat, J.K. Pandey, A. Kumar, R. Gupta, A review on fundamentals, constraints and fabrication techniques of superhydrophobic coatings, Progress In Organic Coatings, 142 (2020). https://10.1016/j.porgcoat.2020.105557

[18] J.T. Chen, S. Ahmad, J.J. Cai, H.Q. Liu, K.T. Lau, J.Y. Zhao, Latest progress on nanotechnology aided boiling heat transfer enhancement: A review, Energy, 215 (2021). https://doi.org/10.1016/j.energy.2020.119114

[19] T.A. Saleh, N. Baig, Efficient chemical etching procedure for the generation of superhydrophobic surfaces for separation of oil from water, Progress In Organic Coatings, 133 (2019) 27-32. https://doi.org/10.1016/j.porgcoat.2019.03.049

[20] J.H. Kim, A. Mirzaei, H.W. Kim, S.S. Kim, Facile fabrication of superhydrophobic surfaces from austenitic stainless steel (AISI 304) by chemical etching, Applied Surface Science, 439 (2018) 598-604. https://doi.org/10.1016/j.apsusc.2017.12.211

[21] B. Farshchian, J. Pierce, M.S. Beheshti, S. Park, N. Kim, Droplet impinging behavior on surfaces with

wettability contrasts, Microelectronic engineering, 195 (2018) 50-56. https://doi.org/10.1016/j.mee.2018.03.019
[22] S. Sikalo, M. Marengo, C. Tropea, E.N. Ganic, Analysis of impact of droplets on horizontal surfaces, Experimental Thermal And Fluid Science, 25 (2002) 503-510. https://doi.org/10.1016/S0894-1777(00)00109-1
[23] S.J. Lin, B.Y. Zhao, S. Zou, J.W. Guo, Z. Wei, L.Q. Chen, Impact of viscous droplets on different wettable surfaces: Impact phenomena, the maximum spreading factor, spreading time and post-impact oscillation, Journal Of Colloid And Interface Science, 516 (2018) 86-97. https://doi.org/10.1016/j.jcis.2017.12.086
[24] H. Kim, U. Park, C. Lee, H. Kim, M.H. Kim, J. Kim, Drop splashing on a rough surface: How surface morphology affects splashing threshold, Appl Phys Lett, 104 (2014). https://doi.org/10.1063/1.4873338
[25] J. Qu, Y.L. Yang, S.S. Yang, D.H. Hu, H.H. Qiu, Droplet impingement on nano-textured superhydrophobic surface: Experimental and numerical study, Applied Surface Science, 491 (2019) 160-170. https://doi.org/10.1016/j.apsusc.2019.06.104
[26] C.C. Yin, T.Y. Wang, Z.Z. Che, M. Jia, K. Sun, Oblique impact of droplets on microstructured superhydrophobic surfaces, International Journal Of Heat And Mass Transfer, 123 (2018) 693-704. https://doi.org/10.1016/j.ijheatmasstransfer.2018.02.060
[27] G.T. Liang, I. Mudawar, Review of drop impact on heated walls, International Journal Of Heat And Mass Transfer, 106 (2017) 103-126. https://doi.org/10.1016/j.ijheatmasstransfer.2016.10.031
[28] L. Guo, Y.H. Gao, N.N. Cai, D.G. Li, Y.Y. Yan, W.C. Sun, Morphological Development of Fuel Droplets after Impacting Biomimetic Structured Surfaces with Different Temperatures, J Bionic Eng, 17 (2020) 822-834. https://doi.org/10.1007/s42235-020-0050-3
[29] S.C. Wong, Y.C. Lin, Effect of copper surface wettability on the evaporation performance: Tests in a flat-plate heat pipe with visualization, International Journal Of Heat And Mass Transfer, 54 (2011) 3921-3926. https://doi.org/10.1016/j.ijheatmasstransfer.2011.04.033
[30] T. Tran, H.J.J. Staat, A. Susarrey-Arce, T.C. Foertsch, A. van Houselt, H. Gardeniers, A. Prosperetti, D.

Lohse, C. Sun, Droplet impact on superheated micro-structured surfaces, Soft Matter, 9 (2013) 3272-3282. https://doi.org/10.1039/c3sm27643k

[31] V.O. Ng, H. Yu, H.A. Wu, Y.M. Hung, Thermal performance enhancement and optimization of two-phase closed thermosyphon with graphene-nanoplatelets coatings, Energy Conv. Manag., 236 (2021) 14. https://doi.org/10.1016/j.enconman.2021.114039

[32] J. Li, L. Lv, G. Zhou, X. Li, Mechanism of a microscale flat plate heat pipe with extremely high nominal thermal conductivity for cooling high-end smartphone chips, Energy Conv. Manag., 201 (2019) 112202. https://doi.org/10.1016/j.enconman.2019.112202

[33] W.B. Zhou, X.G. Hu, Y. He, Y.Y. Yu, L. Mao, Study on axial wetting length and evaporating heat transfer in rectangular microgrooves with superhydrophilic nano-textured surfaces for two-phase heat transfer devices, Energy Conv. Manag., 200 (2019) 14. https://doi.org/10.1016/j.enconman.2019.112098

[34] J. Shen, C. Graber, J. Liburdy, D. Pence, V. Narayanan, Simultaneous droplet impingement dynamics and heat transfer on nano-structured surfaces, Experimental Thermal And Fluid Science, 34 (2010) 496-503. https://doi.org/10.1016/j.expthermflusci.2009.02.003

[35] I.U. Vakarelski, N.A. Patankar, J.O. Marston, D.Y.C. Chan, S.T. Thoroddsen, Stabilization of Leidenfrost vapour layer by textured superhydrophobic surfaces, Nature, 489 (2012) 274-277. https://doi.org/10.1038/nature11418

[36] S.H. Joghee, K.M. Uthandi, N. Singh, S. Katti, P. Kumar, R.K. Renganayagalu, B. Pullithadathil, Evolution of Temperature-Driven Interfacial Wettability and Surface Energy Properties on Hierarchically Structured Porous Superhydrophobic Pseudoboehmite Thin Films, Langmuir, 36 (2020) 6352-6364. https://doi.org/10.1021/acs.langmuir.0c00368

[37] R. Wu, O. Lamini, C.Y. Zhao, Leidenfrost temperature: Surface thermal diffusivity and effusivity effect, International Journal Of Heat And Mass Transfer, 168 (2021).

https://doi.org/10.1016/j.ijheatmasstransfer.2020.120892

[38] C.E. Clavijo, J. Crockett, D. Maynes, Hydrodynamics of droplet impingement on hot surfaces of varying wettability, International Journal Of Heat And Mass Transfer, 108 (2017) 1714-1726. https://doi.org/10.1016/j.ijheatmasstransfer.2016.12.076

[39] K. Chen, R.N. Xu, P.X. Jiang, Evaporation Enhancement of Microscale Droplet Impact on Micro/Nanostructured Surfaces, Langmuir, 36 (2020) 12230-12236. https://doi.org/10.1021/acs.langmuir.0c01975

[40] G. Lagubeau, M. Le Merrer, C. Clanet, D. Quere, Leidenfrost on a ratchet, Nat Phys, 7 (2011) 395-398. https://doi.org/10.1038/NPHYS1925

[41] I.U. Vakarelski, J.O. Marston, D.Y.C. Chan, S.T. Thoroddsen, Drag Reduction by Leidenfrost Vapor Layers, Phys Rev Lett, 106 (2011). https://doi.org/10.1103/PhysRevLett.106.214501

[42] M.Y. Chen, Z.H. Jia, T. Zhang, Y.Y. Fei, Self-propulsion of Leidenfrost droplets on micropillared hot surfaces with gradient wettability, Applied Surface Science, 433 (2018) 336-340. https://doi.org/

[43] L.S. Zhong, Z.G. Guo, Effect of surface topography and wettability on the Leidenfrost effect, Nanoscale, 9 (2017) 6219-6236. https://doi.org/10.1039/c7nr01845b

[44] G.C. Lee, J.Y. Kang, H.S. Park, K. Moriyama, S.H. Kim, M.H. Kim, Induced liquid-solid contact via micro/nano multiscale texture on a surface and its effect on the Leidenfrost temperature, Experimental Thermal And Fluid Science, 84 (2017) 156-164. https://doi.org/10.1016/j.expthermflusci.2017.01.022

[45] S.Y. Misyura, The effect of Weber number, droplet sizes and wall roughness on crisis of droplet boiling, Experimental Thermal And Fluid Science, 84 (2017) 190-198. https://10.1016/j.expthermflusci.2017.02.014

[46] H.M. Kwon, J.C. Bird, K.K. Varanasi, Increasing Leidenfrost point using micro-nano hierarchical surface structures, Appl Phys Lett, 103 (2013). https://doi.org/10.1063/1.4828673

[47] H. Nair, H.J.J. Staat, T. Tran, A. van Houselt, A. Prosperetti, D. Lohse, C. Sun, The Leidenfrost temperature

increase for impacting droplets on carbon-nanofiber surfaces, Soft Matter, 10 (2014) 2102-2109. https://doi.org/10.1039/c3sm52326h

[48] S.H. Kim, Y.Y. Jiang, H. Kim, Droplet impact and LFP on wettability and nanostructured surface, Experimental Thermal And Fluid Science, 99 (2018) 85-93. https://doi.org/10.1016/j.expthermflusci.2018.07.029

[49] R. Hays, D. Maynes, J. Crockett, Thermal transport to droplets on heated superhydrophobic substrates, International Journal Of Heat And Mass Transfer, 98 (2016) 70-80. https://doi.org/10.1016/j.ijheatmasstransfer.2016.03.011

[50] Q. Ma, X.M. Wu, T. Li, F.Q. Chu, Droplet boiling on heated surfaces with various wettabilities, Appl Therm Eng, 167 (2020) 8. https://doi.org/10.1016/j.applthermaleng.2019.114703

[51] O. Dubnack, C. Kunz, S. Graf, F.A. Muller, Laser-induced Leidenfrost surfaces, Applied Surface Science, 532 (2020). https://10.1016/j.apsusc.2020.147407

[52] M.A.J. van Limbeek, O. Ramirez-Soto, A. Prosperetti, D. Lohse, How ambient conditions affect the Leidenfrost temperature, Soft Matter, 17 (2021) 3207-3215. https://doi.org/10.1039/d0sm01570a

[53] L.R. Villegas, S. Tanguy, G. Castanet, O. Caballina, F. Lemoine, Direct numerical simulation of the impact of a droplet onto a hot surface above the Leidenfrost temperature, International Journal Of Heat And Mass Transfer, 104 (2017) 1090-1109. https://doi.org/10.1016/j.ijheatmasstransfer.2016.08.105

[54] W.X. Li, Q. Li, Y. Yu, Z.X. Wen, Enhancement of nucleate boiling by combining the effects of surface structure and mixed wettability: A lattice Boltzmann study, Appl Therm Eng, 180 (2020) 11. https://doi.org/10.1016/j.applthermaleng.2020.115849

[55] A. Tuoliken, L.P. Zhou, P. Bai, X.Z. Du, On the Leidenfrost effect of water droplet impacting on superalloy plate surface, International Journal Of Heat And Mass Transfer, 172 (2021).

https://doi.org/10.1016/j.ijheatmasstransfer.2021.121218